 Printed in China Communications in Theoretical Physics

Commun. Theor. Phys. **77** (2025) 015402 (13pp) https://doi.org/10.1088/1572-9494/ad7831

Plasma impact on black hole shadows and gravitational weak lensing in the Einstein–Maxwell-scalar theory

Mirzabek Alloqulov[1,2,3], **Sanjar Shaymatov**[4,1,5,6], **Abdul Jawad**[4,7] and **Oripjon Zaripov**[5]

[1] Institute of Fundamental and Applied Research, National Research University TIIAME, Kori Niyoziy 39, Tashkent 100000, Uzbekistan
[2] University of Tashkent for Applied Sciences, Str. Gavhar 1, Tashkent 100149, Uzbekistan
[3] Shahrisabz State Pedagogical Institute, Shahrisabz Str. 10, Shahrisabz 181301, Uzbekistan
[4] Institute for Theoretical Physics and Cosmology, Zhejiang University of Technology, Hangzhou 310023, People's Republic of China
[5] Tashkent State Technical University, Tashkent 100095, Uzbekistan
[6] Western Caspian University, Baku AZ1001, Azerbaijan
[7] Department of Mathematics, COMSATS University Islamabad, Lahore Campus, Lahore-54000, Pakistan

E-mail: malloqulov@gmail.com, sanjar@astrin.uz, jawadab181@yahoo.com and o.zaripov@edu.uz

Received 8 June 2024, revised 28 August 2024
Accepted for publication 9 September 2024
Published 8 November 2024

Abstract

In this paper, we investigate the optical properties of a non-rotating charged black hole (BH) in the Einstein–Maxwell-scalar (EMS) theory, together with a plasma medium. We first consider the photon sphere and shadow radius under the impact of the plasma medium existing in the environment surrounding the BH in the EMS theory. We show that the radius of the photon sphere and the BH shadow decrease under the influence of the parameter β. We further study gravitational weak lensing in detail by adapting general methods and derive the light ray's deflection angle around the BH together with the plasma environment. It is found that for uniform plasma, the deflection angle increases with the rise of the plasma parameter, whereas it decreases with the increase of the plasma parameter for non-uniform plasma. Besides, we also study the magnification of image brightness.

Keywords: general relativity, black hole shadow, gravitational weak lensing

(Some figures may appear in colour only in the online journal)

1. Introduction

In general relativity (GR), black holes (BHs) were initially predicted to be formed by the gravitational collapse of compact massive bodies, usually referred to as solutions to the field equations of GR. However, the modern observations, such as recent gravitational wave detectors [1, 2] and the BlackHoleCam and EHT collaborations [3, 4], have confirmed their existence in the Universe, opening attractive avenues for future research to examine important insights remarkable properties of BHs in GR. Observations have also predicted that BHs can be considered rotating black holes [5–10]. Hence, BHs can at least possess mass M and spin a. However, BHs can also have an electric charge that was proposed by various mechanisms, such as the balance of gravitational and Coulomb forces [11, 12] and the irradiating photons [13], which may provide a positive net electric charge at the near surface of BHs. Additionally, magnetic field lines can lead to a induced charge under the Wald mechanism due to the frame dragging effect [14]. Then the exact solution of the rotating Schwinger dyon was obtained in the form of a charged BH with mass M and electric and magnetic charges, together with spin a [15, 16]. Furthermore, solutions of charged BHs without physical singularity were proposed as regular BH solutions with nonlinear electrodynamics (NED) and extended to various contexts [17–27]. It

is worth noting that GR was successfully tested in addressing the low energy limit of string theory with the dilaton scalar field presented by the Einstein–Hilbert action as a combination of the axion, gauge and dilaton fields [28, 29]. Later, the heterotic string theory with the scalar dilaton field associated with the electromagnetic field tensor was also proposed in [30]. This also led to an increase in activity where various authors investigated the causal structures and thermodynamic properties of BH solutions with dilaton field in various scenarios [29–34]. Additionally, there are investigations that suggested a means of obtaining BH solutions within the string theory and extended theories [35–39]. Later on, the quantum aspects have also been considered in BH solutions, and their effects on the background geometry have been examined in the context of extended theories of gravity [40–44].

The EHT collaboration [3, 4] first reported a BH's image/shadow recently. With the recent discovery of BH images/shadows, many researchers have been focusing on theoretical modeling of BH shadows. It is envisaged by the fact that the light can be highly bent and even travels in circles near the BH, as no light escapes from the BH, resulting in the BH appearing as a dark disk, usually referred to as the BH's shadow. The point to be noted is that the first study of the light bending around the Schwarzschild BH was conducted by Synge [45], and later its image was simulated by Luminet [46]. In this context, the study of the light bending and the shadow analysis allow one to test the spacetime geometry with its accretion disk. To this end, Amarilla et al first conducted the shadow analysis for a Kaluza–Klein rotating dilaton BH [47]. Following this analysis, it was then extended to the Einstein–Maxwell–Dilaton–Axion BH [48]. The BH shadow was also examined around the rotating charged BH including a scalar dilaton field [49]. An investigation also exists showing that the BH shadow can be significantly influenced by the impact of the deformation parameters [50]. Also, the BH shadow analysis can be applied for scalar boson and Proca stars, showing the geometry of such alternative compact objects that may exhibit departures from BH geometries [51–53]. Other theoretical modeling of BH shadows have also been proposed in recent years, and thus it has sparked increased research activity, with various authors investigating BH shadows in different scenarios [54–69].

It must also be emphasized that, together with BH shadow analysis, the gravitational lensing plays a decisive role in probing unknown aspects of astrophysical compact objects. It is envisaged that the light can be highly deflected, thus changing its path around a BH. This deflection reflects the gravitational lensing in GR. This is because GR was widely examined first through the gravitational lensing effects [70]. Therefore, gravitational lensing can allow one to test the background geometry at the BH's close vicinity and provide information regarding distant sources and compact objects. Additionally, it may provide the possibility to exhibit departures in the geometry and structure of astrophysical compact objects. This also led to an increase in activity, where various authors have been extending the gravitational lensing effects to examine theories of gravity in various situations [see, e.g. [71–80]]. Additionally, an extensive analysis has been implemented on these lines to study gravitational lensing effects in the weak-field regime in the presence of a plasma medium [81–87] and in the context of modified theories of gravity [88–90].

It is believed that the plasma medium can exist in the environment surrounding a BH in the astrophysical scenario. As stated, BHs are very intriguing gravitational and geometric objects that showcase regions where spatial curvature dominates the description of gravity. Therefore, it would be valuable to explore BHs in different contexts, including in EMS theory. In this regard, investigating a solution describing a charged BH in EMS theory as an extension of the Reissner–Nordström (RN) solution involving a dilaton field could provide an interesting alternative for testing optical phenomena in strong gravity field regimes. This solution in EMS theory offers unique features compared to the Schwarzschild BH in Einstein's theory and other dilaton BH solutions. Therefore, studying BHs in EMS theory with a plasma medium and examining their effects on optical phenomena can enhance our understanding of its optical properties and provide insights into deviations from other BH solutions in astrophysical observations. In this paper, our research not only contributes to theoretical knowledge but also sets the stage for future observational and experimental endeavor to investigate extreme environments around BHs. With this motivation, in this paper, we consider an interesting solution describing a charged black hole in the EMS theory of gravity, together with its properties. We aim to study the shadow and gravitational lensing effects, including the magnification of lensed images in the presence of the plasma medium. We then investigate the plasma effects along with the BH parameters on these astrophysical events, enhancing our understanding of their implications in explaining astrophysical observations.

The paper is organized as follows. We briefly review the solution of the charged BH in EMS theory, together with the photon motion and its dynamics, which is followed by the study of the BH shadow in the presence of plasma medium in section 2. Further, we consider the weak gravitational lensing in section 3 and the magnification of the gravitationally lensed images in section 4 in the presence of the plasma medium. We summarize our results in section 5. Throughout this paper, we use $(-, +, +, +)$ signature for the spacetime metric and system of units in which we set $G = c = 1$.

2. Plasma impact on black hole shadow

2.1. Charged black hole in Einstein–Maxwell-scalar theory

Here, we consider the metric that can describe a static charged BH in EMS theory in Schwarzschild coordinates (t, r, θ, ϕ) can be written as (see details in [29, 91])

$$S = \int \mathrm{d}^4x\sqrt{-g}\,[R - 2\nabla_\alpha\phi\nabla^\alpha\phi - K(\phi)F_{\alpha\beta}F^{\alpha\beta} - V(\phi)],$$

where ϕ is the massless scalar field and $K(\phi)$ the scalar field function in the action and $K(\phi)$ the coupling function acting as the relation for the electromagnetic $F_{\alpha\beta}$ and dilaton fields. Note that the term $V(\phi)$ is the potential associated with

the cosmological constant Λ, $V(\phi) = \frac{\Lambda}{3}(e^{2\phi} + 4 + e^{-2\phi})$, usually referred to as the de-Sitter BH solution including the dilaton field in the EMS theory [92]. We can then further consider the case, $V(\phi) = 0$, which allows one to describe a spherically symmetric charged BH as follows [91]

$$ds^2 = -U(r)dt^2 + \frac{dr^2}{U(r)} + f(r)(d\theta^2 + \sin^2\theta d\varphi^2), \quad (1)$$

where $U(r)$ and $f(r)$ are defined by

$$f(r) = r^2\left(1 + \frac{\gamma Q^2}{Mr}\right),$$
$$U(r) = 1 - \frac{2M}{r} + \frac{\beta Q^2}{f(r)}, \quad (2)$$

where M is the mass and Q is the BH's electric charge. The radial functions $U(r)$ and $f(r)$ include dimensionless constants such as β and γ in the EMS theory. It can be straightforward that one can recover the Schwarzschild and the RN BH solutions from $f(r)$ and $U(r)$ depending on parameters β and γ [29, 30], e.g. the solution with $\beta \to 0$ and $\gamma \to 0$ reduces to the Schwarzschild, $\gamma = 0$ and $\beta = 1$ to the Reissner–Nordström and $\beta = 0$ and $\gamma = -1$ to the dilation BH solutions [93, 94]. We further wish to examine the null geodesics around the charged EMS black hole in the presence of plasma medium.

To this end, we consider the photon motion and its dynamics with the usage of the Hamilton–Jacobi equation. Hence, we need to write the Hamiltonian for the null geodesics around the BH with the plasma distribution background, i.e., it is given by [95]

$$\mathcal{H}(x^\alpha, p_\alpha) = \frac{1}{2}[g^{\alpha\beta}p_\alpha p_\beta - (n^2 - 1)(p_\beta u^\beta)^2], \quad (3)$$

where x^α is the spacetime coordinates, u^β and p_α the four-velocity and momentum of the photon. Note that, in equation (3), n is the refractive index, i.e., $n = \omega/k$ with k the wave number, which can be written as [96]

$$n^2 = 1 - \frac{\omega_p^2}{\omega^2}, \quad (4)$$

with plasma frequency $\omega_p^2(x^\alpha) = 4\pi e^2 N(x^\alpha)/m_e$, where m_e and e are the electron mass and charge and N the number density of the electrons. Following $\omega^2 = (p_\beta u^\beta)^2$, the photon frequency, ω, can then be defined by

$$\omega(r) = \frac{\omega_0}{\sqrt{U(r)}}, \qquad \omega_0 = \text{const.} \quad (5)$$

For the metric function, $U(r) \to 1$ is satisfied as $r \to \infty$ and $\omega(\infty) = \omega_0 = -p_t$ that manifests the photon energy at spatial infinity [97]. Using the photon geodesics $\mathcal{H} = 0$, ω_0 can be restricted as follows:

$$\frac{\omega_0^2}{U(r)} > \omega_p^2(r). \quad (6)$$

The physical meaning of this restriction is that the photon frequency at a given point, $\omega(r)$, must be greater than the plasma frequency at the same point. This rule consistently applies to light propagation in a plasma. Therefore, the BH shadow can have various forms compared to the vacuum case, i.e., $\omega_p = 0$. For the light geodesics in the presence of a plasma medium the Hamiltonian then yields as [95, 98]

$$\mathcal{H} = \frac{1}{2}[g^{\alpha\beta}p_\alpha p_\beta + \omega_p^2]. \quad (7)$$

The light ray equations for the photon then take the following forms in the equatorial plane $\theta = \pi/2$

$$\dot{t} \equiv \frac{dt}{d\lambda} = \frac{-p_t}{U(r)}, \quad (8)$$

$$\dot{r} \equiv \frac{dr}{d\lambda} = p_r U(r), \quad (9)$$

$$\dot{\phi} \equiv \frac{d\phi}{d\lambda} = \frac{p_\phi}{f(r)}, \quad (10)$$

with the relation $\dot{x}^\alpha = \partial\mathcal{H}/\partial p_\alpha$. We use equations (9) and (10) to obtain the orbit equation as follows:

$$\frac{dr}{d\phi} = \frac{g^{rr}p_r}{g^{\phi\phi}p_\phi}. \quad (11)$$

For the photon geodesics $\mathcal{H} = 0$, the above equation can yield

$$\frac{dr}{d\phi} = \sqrt{\frac{g^{rr}}{g^{\phi\phi}}}\sqrt{\gamma^2(r)\frac{\omega_0^2}{p_\phi^2} - 1}, \quad (12)$$

where the following relation holds well

$$\gamma^2(r) \equiv -\frac{g^{tt}}{g^{\phi\phi}} - \frac{\omega_p^2}{g^{\phi\phi}\omega_0^2}. \quad (13)$$

For a light ray that comes from infinity, reaches a minimum at a radius r_{ps}, and goes out to infinity again. From a mathematical point of view, it is a turning point of the $\gamma^2(r)$ function. Therefore, the radius of the photon sphere can be determined from the following equation

$$\frac{d(\gamma^2(r))}{dr}\bigg|_{r=r_{ps}} = 0. \quad (14)$$

The above equation solves to give the photon radii that we further explore numerically. In figure 1, we depict the photon radii for various possible cases. It can be observed from figure 1 that the radius of the photon sphere always increases in size with the increase in plasma frequency, while it decreases with the increase in the BH charge Q. It should also be noted that the curves of the photon radius sphere shift down to its small values as the parameter β increases. They do however shift up to its larger values under the effect of the parameter γ, depending on its sign, as seen in the top-right panel of figure 1.

2.2. Black hole shadow in plasma

Now we consider the radius of the shadow of the charged BH in the presence of plasma. To be more informative, we show the trajectory of the photon in figure 2. It can be seen from figure 2 that the angle α approaches the angular radius of the shadow, α_{sh}, as $R \to r_{ps}$. On the usage of this figure, we can

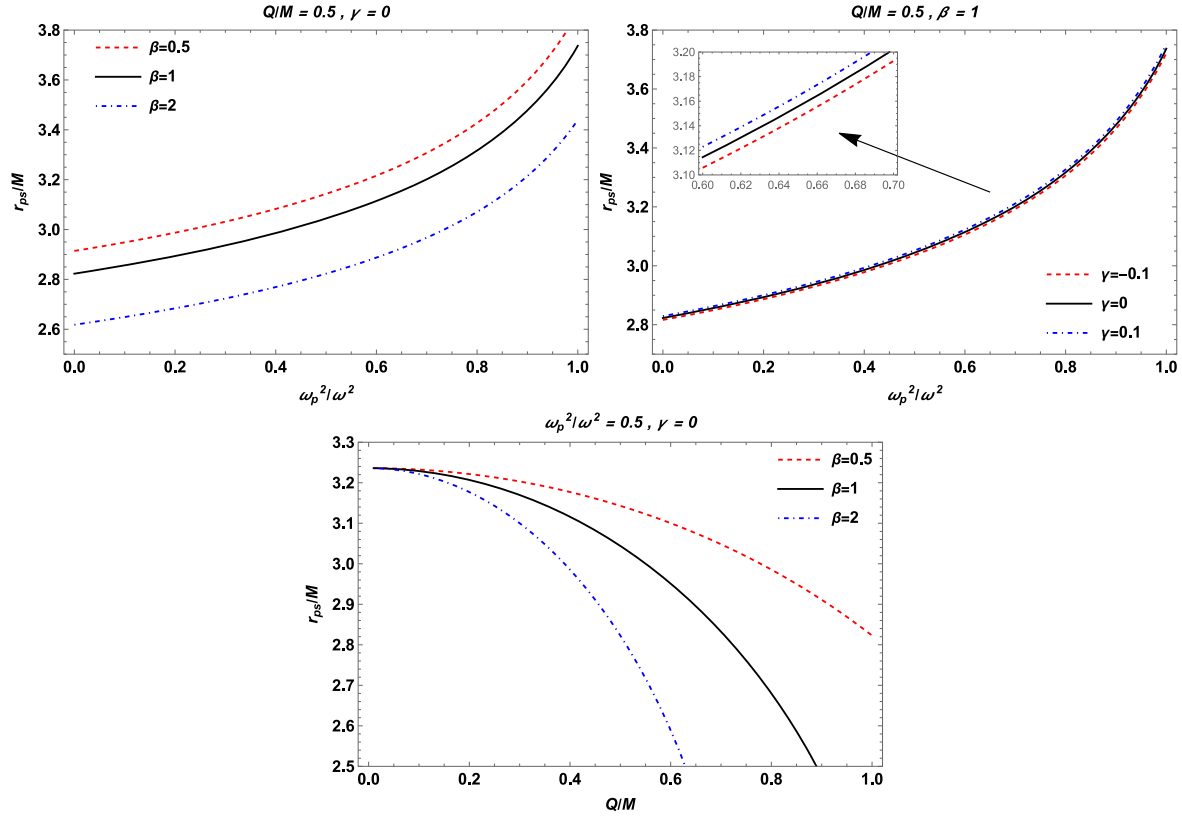

Figure 1. Top-left panel: the dependence of the radius of the photon sphere on the plasma frequency for different values of the β parameter. BH charge and γ parameter are $Q/M = 0.5$ and $\gamma = 0$, respectively. Top-right panel: the radius of the photon sphere as a function of the plasma frequency for different values of the γ parameter. BH charge and β parameter are $Q/M = 0.5$ and $\beta = 1$, respectively. Bottom panel: the dependence of the radius of the photon sphere on the BH charge for different values of the β parameter. The other parameters are $\omega_{\rm p}^2/\omega^2 = 0.5$ and $\gamma = 0$.

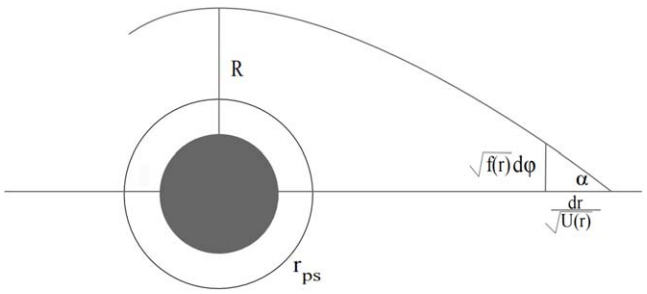

Figure 2. The angle α approaches the angular radius of the BH shadow $\alpha_{\rm sh}$ as R approaches $r_{\rm ps}$.

further explore the BH shadow. The angular radius $\alpha_{\rm sh}$ of the BH can be defined as [55, 97]

$$\sin^2\alpha_{\rm sh} = \frac{\gamma^2(r_{\rm ps})}{\gamma^2(r_{\rm o})}, = \frac{f(r_{\rm ps})\left[\frac{1}{U(r_{\rm ps})} - \frac{\omega_p^2(r_{\rm ps})}{\omega_0^2}\right]}{f(r_{\rm o})\left[\frac{1}{U(r_{\rm o})} - \frac{\omega_p^2(r_{\rm o})}{\omega_0^2}\right]}, \quad (15)$$

where $r_{\rm ps}$ and $r_{\rm o}$ represent the locations of the photon sphere and the observer, respectively. From equation (13) we can easily find the $\gamma^2(r_{\rm ps})$ and $\gamma^2(r_o)$. If the observer is located at a sufficiently large distance from the BH then it can be approximated the radius of BH shadow using equation (15) as [97]

$$R_{\rm sh} \simeq r_{\rm o}\sin\alpha_{\rm sh}, = \sqrt{f(r_{\rm ps})\left[\frac{1}{U(r_{\rm ps})} - \frac{\omega_{\rm p}^2(r_{\rm ps})}{\omega_0^2}\right]}, \quad (16)$$

where we have used the fact that $\gamma(r) \to r$, which follows from equation (13), at spatial infinity for both models of plasma along with a constant magnetic field. The top-left panel of figure 3 shows the dependence of the BH shadow on the plasma frequency for different values of the β parameter. One can see from this figure that the radius of the BH shadow decreased with an increase of the plasma frequency. Also, under the influence of the β parameter the radius of the BH shadow decreased. It can be seen from the top-right panel of this figure that the radius of the BH shadow depends on the sign of the γ parameter. Similarly, the radius of the BH shadow decreased with an increase of the BH charge as demonstrated in the bottom panel of figure 3. Now we consider the assumption that the compact objects Sgr A* and M87* are static, spherically symmetric objects, even though the observation obtained by the EHT collaboration does not support the assumption made here. However, we try to theoretically investigate the lower limits of the BH charge Q of the BH in EMS theory, using the data provided by the EHT

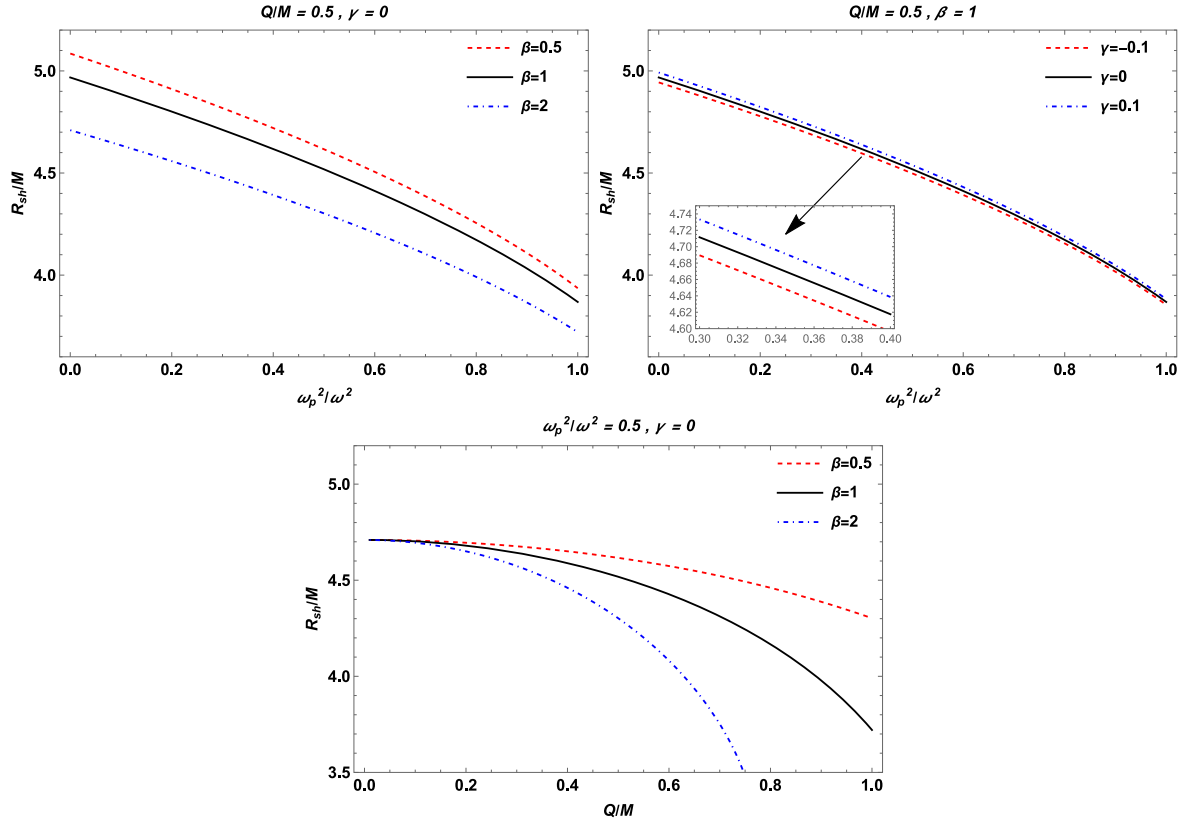

Figure 3. Top-left panel: the dependence of the radius of the BH shadow on the plasma frequency for different values of the β parameter. BH charge and γ parameter are $Q/M = 0.5$ and $\gamma = 0$, respectively. Top-right panel: the radius of the BH shadow as a function of the plasma frequency for different values of the γ parameter. BH charge and β parameter are $Q/M = 0.5$ and $\beta = 1$, respectively. Bottom panel: the dependence of the radius of the BH shadow on the BH charge for different values of the β parameter. The other parameters are $\omega_{\rm p}^2/\omega^2 = 0.5$ and $\gamma = 0$.

collaboration project. For constraint, we chose the BH charge Q and the plasma frequency. One can use the observational data provided by the EHT collaboration regarding the shadows of the supermassive black holes Sgr A* and M87* in order to constrain these two quantities Q and ω_p^2/ω^2. The angular diameter $\theta_{\rm M87^*}$ of the BH shadow, the distance from Earth and the mass of the BH at the center of the M87* are $\theta_{\rm M87^*} = 42 \pm 3\mu as$, $D = 16.8 \pm 0.8$ Mpc and $M_{\rm M87^*} = 6.5 \pm 0.7 \times 10^9 M_\odot$ [3], respectively. For Sgr A*, the data provided by the EHT collaboration are $\theta_{\rm SgrA^*} = 48.7 \pm 7\mu$ $D = 8277 \pm 9 \pm 33pc$ and $M_{\rm SgrA^*} = 4.297 \pm 0.013 \times 10^6 M_\odot$ (VLTI) [99]. From this information, we can calculate the diameter of the shadow caused by the compact object per unit mass as follows [100]

$$d_{\rm sh} = \frac{D\theta}{M}. \tag{17}$$

We know that from the expression $d_{\rm sh} = 2R_{\rm sh}$, we can easily obtain the expression for the diameter of the BH shadow. It is worth noting that the distance D is considered a dimension of M [3, 4]. Thus, the diameter of the BH shadow $d_{\rm sh}^{\rm M87^*} = (11 \pm 1.5)$M for M87* and $d_{\rm sh}^{\rm Sgr^*} = (9.5 \pm 1.4)$M for Sgr A*. From observational EHT data, we can find the lower limits on the quantities Q and $\omega_{\rm p}^2/\omega^2$ for the supermassive BHs at the centers of the galaxies Sgr A* and M87*. It is demonstrated numerically in figure 4.

3. Weak gravitational lensing for black hole

Here, we consider the weak gravitational lensing for uniform and non-uniform plasma cases. For that we first represent a weak-field approximation that is defined by [75, 101]

$$g_{\alpha\beta} = \eta_{\alpha\beta} + h_{\alpha\beta}, \tag{18}$$

where $\eta_{\alpha\beta}$ and $h_{\alpha\beta}$ are respectively introduced to define the expressions for Minkowski spacetime and the perturbation gravity field that delineates the EMS theory and is defined by

$$\begin{aligned} &\eta_{\alpha\beta} = {\rm diag}(-1, 1, 1, 1), \\ &h_{\alpha\beta} \ll 1, \, h_{\alpha\beta} \to 0 {\rm under} x^\alpha \to \infty, \\ &g^{\alpha\beta} = \eta^{\alpha\beta} - h^{\alpha\beta}, \, h^{\alpha\beta} = h_{\alpha\beta}. \end{aligned} \tag{19}$$

Following to the fundamental equation we are able to

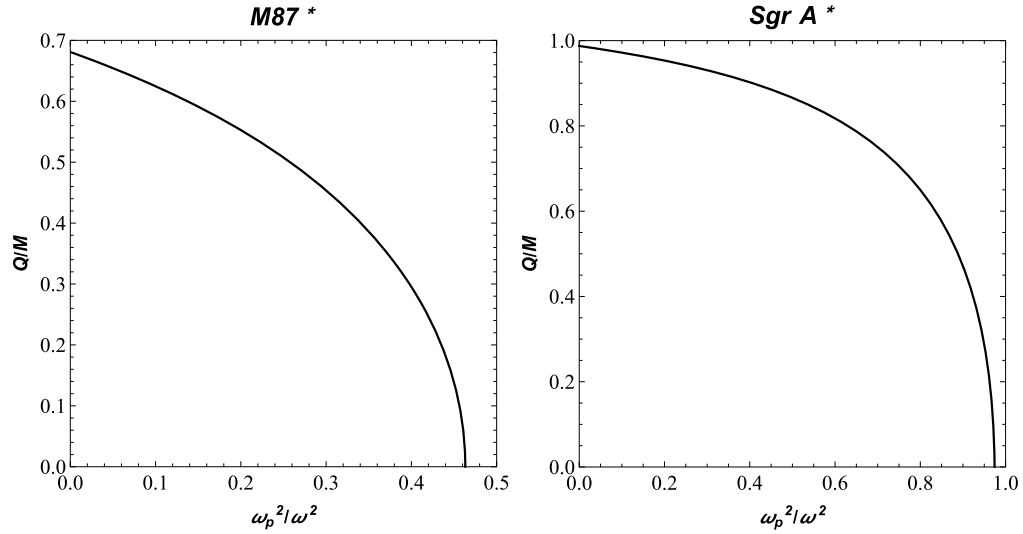

Figure 4. The constrained values of BH charge Q and $\omega_{\rm p}^2/\omega_0^2$ for supermassive BHs sitting at the center M87 and Sgr A* galaxies. Here, we note that we set $\beta = 1$ and $\gamma = 0$ for both panels.

represent the deflection angle around the EMS BH as follows [101]

$$\hat{\alpha}_{\rm b} = \frac{1}{2}\int_{-\infty}^{\infty} \frac{b}{r}\left(\frac{{\rm d}h_{33}}{{\rm d}r} + \frac{1}{1-\omega_{\rm p}^2/\omega^2}\frac{{\rm d}h_{00}}{{\rm d}r} - \frac{K_{\rm e}}{\omega^2-\omega_{\rm p}^2}\frac{{\rm d}N}{{\rm d}r}\right){\rm d}z, \tag{20}$$

where ω is the photon frequency and $\omega_{\rm p}$ the plasma frequency. We further expand the metric functions into a Taylor series for calculations. The line element is written as

$${\rm d}s^2 \approx {\rm d}s_0^2 + \left(\frac{2M}{r} - \frac{\beta MQ^2}{r(Mr+\gamma Q^2)}\right){\rm d}t^2 + \left(\frac{2M}{r} - \frac{\beta MQ^2}{r(Mr+\gamma Q^2)}\right){\rm d}r^2, \tag{21}$$

with ${\rm d}s_0^2 = -{\rm d}t^2 + {\rm d}r^2 + r^2({\rm d}\theta^2 + \sin^2\theta {\rm d}\phi^2)$. In the following, we define the components of $h_{\alpha\beta}$ as the perturbations which are written as follows:

$$h_{00} = \frac{2M}{r} - \frac{\beta MQ^2}{r(Mr+\gamma Q^2)}, \tag{22}$$

$$h_{ik} = \left(\frac{2M}{r} - \frac{\beta MQ^2}{r(Mr+\gamma Q^2)}\right)n_i n_k, \tag{23}$$

$$h_{33} = \left(\frac{2M}{r} - \frac{\beta MQ^2}{r(Mr+\gamma Q^2)}\right)\cos^2\chi, \tag{24}$$

with $\cos^2\chi = z^2/(b^2+z^2)$ and $r^2 = b^2 + z^2$. The first derivatives of h_{00} and h_{33} with respect to the radial coordinate then give to write as follows:

$$\frac{{\rm d}h_{00}}{{\rm d}r} = \frac{M(-2M^2r^2 + 2MQ^2r(\beta-2\gamma) + \gamma Q^4(\beta-2\gamma))}{r^2(Mr+\gamma Q^2)^2}, \tag{25}$$

$$\frac{{\rm d}h_{33}}{{\rm d}r} = \frac{Mz^2(-6M^2r^2 + 4MQ^2r(\beta-3\gamma) + 3\gamma Q^4(\beta-2\gamma))}{r^4(Mr+\gamma Q^2)^2}. \tag{26}$$

Taking the above expressions together, the deflection angle can be written as

$$\hat{\alpha_b} = \hat{\alpha_1} + \hat{\alpha_2} + \hat{\alpha_3}, \tag{27}$$

with

$$\hat{\alpha_1} = \frac{1}{2}\int_{-\infty}^{\infty}\frac{b}{r}\frac{{\rm d}h_{33}}{{\rm d}r}{\rm d}z,$$
$$\hat{\alpha_2} = \frac{1}{2}\int_{-\infty}^{\infty}\frac{b}{r}\frac{1}{1-\omega_{\rm p}^2/\omega^2}\frac{{\rm d}h_{00}}{{\rm d}r}{\rm d}z,$$
$$\hat{\alpha_3} = \frac{1}{2}\int_{-\infty}^{\infty}\frac{b}{r}\left(-\frac{K_e}{\omega^2-\omega_{\rm p}^2}\frac{dN}{{\rm d}r}\right){\rm d}z. \tag{28}$$

We further explore the impact of plasma density distributions on the deflection angle. This is what we wish to examine in the following subsections.

3.1. Uniform plasma

Here, we consider a uniform plasma surrounding the BH in EMS theory and examine its impact on the gravitational deflection angle. To this end, we recall equation (27) and rewrite the form of the deflection angle as follows:

$$\hat{\alpha}_{\rm uni} = \hat{\alpha}_{\rm uni1} + \hat{\alpha}_{\rm uni2} + \hat{\alpha}_{\rm uni3}. \tag{29}$$

The use of equations (24), (27) and (28) helps to define the deflection angle influenced by a uniform plasma medium. We then further analyze the deflection angle around the BH in EMS theory. The profile of the deflection angle as a function of the impact parameter b is shown in figure 5 for various combinations of BH charge and parameters β and γ and $\omega_{\rm p}^2/\omega^2$. The left panel reflects the role of parameter β on the deflection angle, whereas the right panel reflects the role of the BH charge while keeping fixed parameters β and γ. As

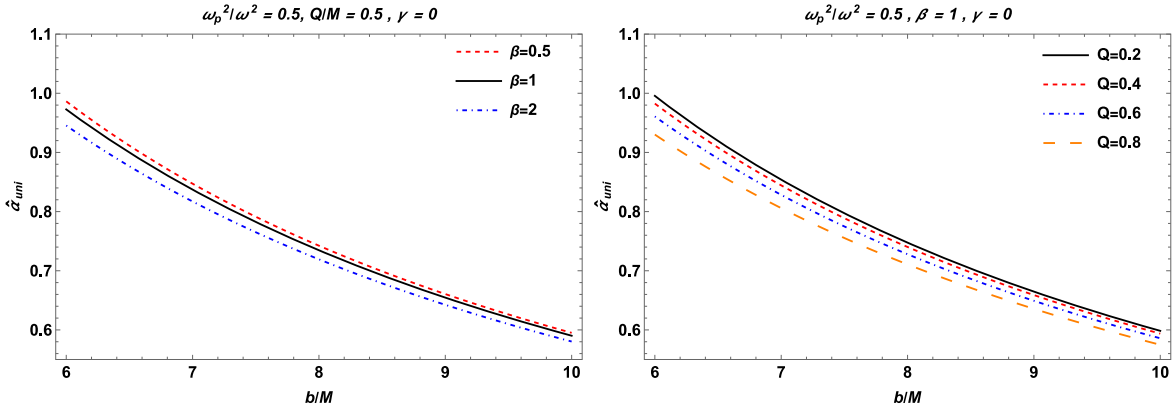

Figure 5. The plots shows the deflection angle $\hat{\alpha}_{\rm uni}$ against the impact parameter b for various combinations of parameter β (left panel) and BH charge Q (right panel).

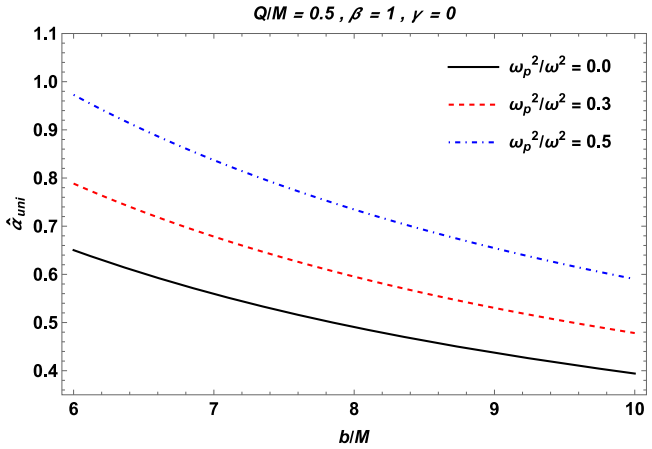

Figure 6. The plot shows the deflection angle $\hat{\alpha}_{\rm uni}$ profile against the impact parameter b for various values of the plasma parameters. Here we have set $Q/M = 0.5$, $\beta = 1$ and $\gamma = 0$.

can observed from figure 5, the deflection angle $\hat{\alpha}_{\rm uni}$, sensitive to the effect of the impact parameter, gets decreased as a consequence of an increase in the values of parameters β and Q. In figure 6, we show the role of the plasma parameters on the deflection angle. It should be noted that the increasing rate of the deflection angle is much more sensitive and increases rapidly as a consequence of an increase in the value of the plasma frequency, as seen in figure 6. As inferred from the increasing rate of the deflection angle, the plasma plays a pivotal role in changing the light geodesics.

3.2. Non-uniform plasma

Here, we consider the non-singular isothermal sphere (SIS) that is the foremost favorable model acting as a useful tool for testing the photon geodesics around BHs, usually referred to as a spherical gas cloud with a singularity sitting at the center of infinite density. SIS density distribution is usually defined by [101]

$$\rho(r) = \frac{\sigma_\nu^2}{2\pi r^2}, \tag{30}$$

where σ_ν^2 represents a one-dimensional velocity dispersion. Keeping this in mind, the analytic expression for the plasma concentration reads as

$$N(r) = \frac{\rho(r)}{km_{\rm p}}, \tag{31}$$

where $m_{\rm p}$ is proton mass and k a dimensionless constant. It is then straightforward to define the plasma frequency as follows:

$$\omega_{\rm e}^2 = K_{\rm e}N(r) = \frac{K_{\rm e}\sigma_\nu^2}{2\pi k m_{\rm p} r^2}. \tag{32}$$

For further analysis of non-uniform plasma (SIS) effect, one needs to write out explicit form for the deflection angle around the BH. It is then written as

$$\hat{\alpha}_{\rm SIS} = \hat{\alpha}_{\rm SIS1} + \hat{\alpha}_{\rm SIS2} + \hat{\alpha}_{\rm SIS3}. \tag{33}$$

The usage of equations (24), (28), and (33) allows one to obtain the form of the deflection angle, as well as to bring out an additional plasma constant ω_c^2 with its explicit form [101]

$$\omega_c^2 = \frac{K_e\sigma_\nu^2}{2\pi k m_{\rm p} R_S^2}, \tag{34}$$

where $R_S = 2M$. In figure 7, we have plotted the behavior of the deflection angle around BH in EMS theory against the impact parameter b for various values of β and Q for fixed γ and $\omega_{\rm p}^2/\omega^2$. One can observe from figure 7 that the deflection angle $\alpha_{\rm sis}$ decreases with the increase in the value of the impact parameter b/M similar to that of the uniform plasma case, while its shape slightly shifts down to its smaller values with increasing the parameter β and the BH charge. It must be noted that the changing rate of the deflection angle may have the opposite behavior as a consequence of the non-uniform plasma effect. For that we turn to analyze the impact of non-uniform plasma on the light's deflection angle, see figure 8. From figure 8 the deflection angle $\alpha_{\rm sis}$ decreases in magnitude with the increase in non-uniform plasma parameter. To gain a deeper understanding in relation to the explicit distinction between the role of the uniform and non-uniform plasma on the light's deflection angle, as seen in figure 9. The light ray's deflection angle acts in a different way, i.e. the uniform and

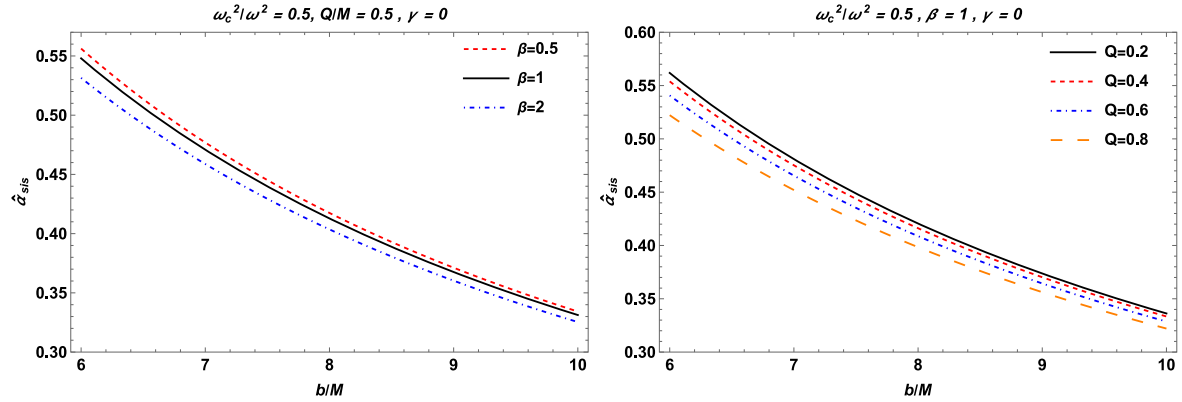

Figure 7. The plot shows the deflection angle $\hat{\alpha}_{\rm sis}$ against the impact parameter b for various values of parameter β (left panel) and BH charge Q (right panel) in the existence of non-uniform plasma.

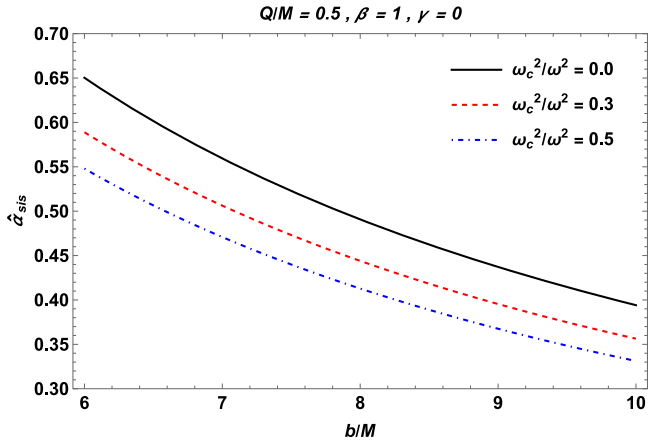

Figure 8. The plot shows the deflection angle $\hat{\alpha}_{\rm sis}$ against the impact parameter b for various values of the plasma parameters. Note that we set $Q/M = 0.5$, $\beta = 1$ and $\gamma = 0$.

non-uniform plasma have the opposite effects on the deflection angle.

4. Magnification of the gravitationally lensed image

Here, we focus on the study of the magnification of the gravitationally lensed image around the BH in EMS theory, placed in the plasma, with the usage of the deflection angle of the light. To this end, we introduce the following equation as a combination of the light angles, $\hat{\alpha_b}$, θ and β around the black hole [71, 75, 102]

$$\theta D_{\rm s} = \beta D_{\rm s} + \hat{\alpha_b} D_{\rm ds}, \tag{35}$$

where $D_{\rm s}$ is the distance between the source and the observer, $D_{\rm d}$ is the lens and the observer, $D_{\rm ds}$ is the source and the lens. Also, θ is the image's angular position and β the source's angular position, respectively. From equation (35), the source's angular position, β, reads as

$$\beta = \theta - \frac{D_{\rm ds}}{D_{\rm s}} \frac{\xi(\theta)}{D_{\rm d}} \frac{1}{\theta}, \tag{36}$$

with $\xi(\theta) = |\hat{\alpha}_b|\, b$ with $b = D_{\rm d}\theta$. It must be noted that the image's shape can be determined as Einstein's ring with the radius $R_{\rm s} = D_{\rm d}\,\theta_{\rm E}$ provided that its appearance is a ring. Here, the corresponding angular part θ_E is given by

$$\theta_E = \sqrt{2R_{\rm s}\frac{D_{ds}}{D_{\rm d}D_{\rm s}}}. \tag{37}$$

The magnification of brightness then yields

$$\mu_\Sigma = \frac{I_{\rm tot}}{I_*} = \sum_k \left| \left(\frac{\theta_k}{\beta}\right)\left(\frac{{\rm d}\theta_k}{{\rm d}\beta}\right) \right|, \quad k = 1, 2, \cdots, j, \tag{38}$$

where $I_{\rm tot}$ is the total brightness and I_* the unlensed brightness of the source, Then, the source's magnification is given by [103–105]

$$\mu_+^{\rm pl} = \frac{1}{4}\left(\frac{x}{\sqrt{x^2+4}} + \frac{\sqrt{x^2+4}}{x} + 2\right), \tag{39}$$

$$\mu_-^{\rm pl} = \frac{1}{4}\left(\frac{x}{\sqrt{x^2+4}} + \frac{\sqrt{x^2+4}}{x} - 2\right), \tag{40}$$

where $x = \beta/\theta_E$ is a dimensionless quantity and $\mu_+^{\rm pl}$ and $\mu_-^{\rm pl}$ the images. As a consequence, the total magnification is given as a liner combination of the images, i.e.,

$$\mu_{\rm tot}^{\rm pl} = \mu_+^{\rm pl} + \mu_-^{\rm pl} = \frac{x^2+2}{x\sqrt{x^2+4}}. \tag{41}$$

Furthermore, we turn to analyze the source's magnification with the usage of two different plasma cases, such as uniform and non-uniform plasma distributions which surround BH in EMS theory. This is what we intend to examine in the next subsections.

4.1. Uniform plasma

In this subsection, we begin to consider the uniform plasma effect on the magnification of the lensed image. Hence, we recall equation (41) with uniform plasma in the EMS BH environment we examine the total magnification of the image, $\mu_{\rm tot}^{\rm pl}$, that reads as

$$\mu_{\rm tot}^{\rm pl} = \mu_+^{\rm pl} + \mu_-^{\rm pl} = \frac{x_{\rm uni}^2+2}{x_{\rm uni}\sqrt{x_{\rm uni}^2+4}}, \tag{42}$$

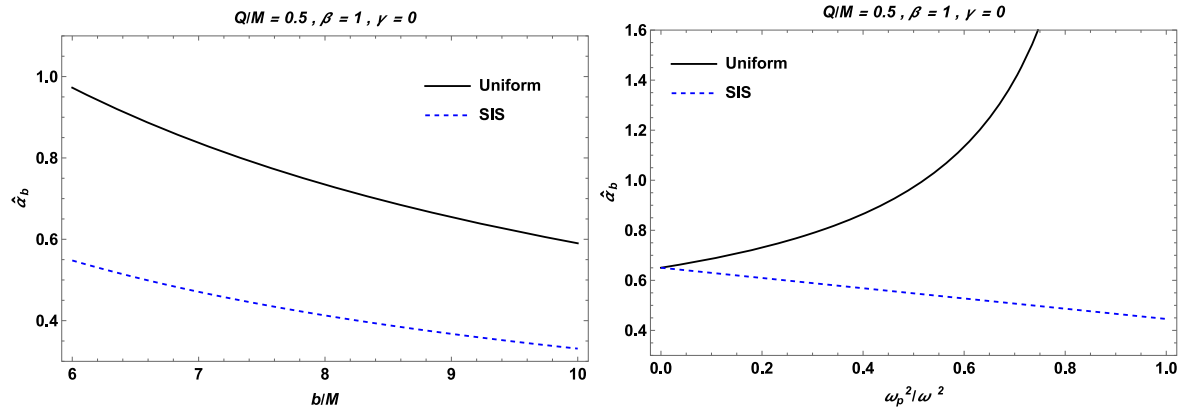

Figure 9. The plot shows the deflection angle $\hat{\alpha}_{\rm b}$ against the impact parameter b (left panel) as well as the plasma parameters $\omega_{\rm p}^2/\omega^2$ (right panel).

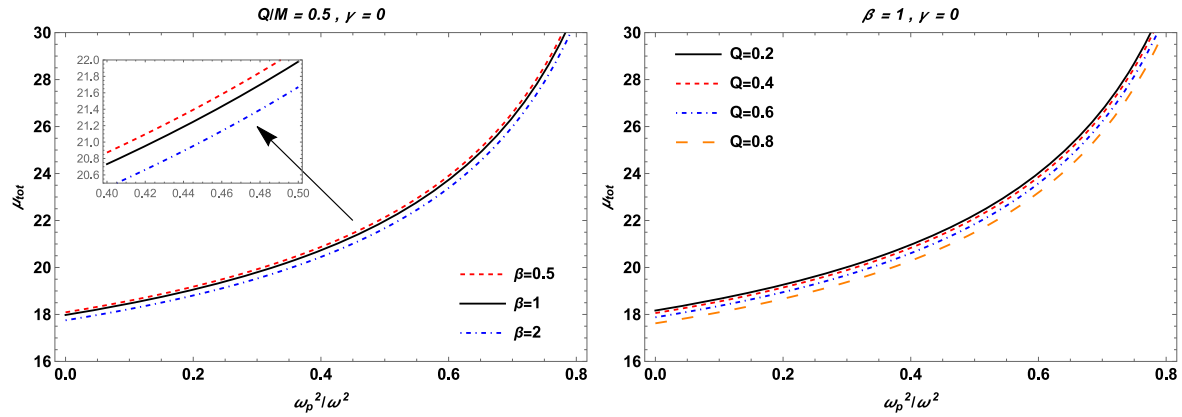

Figure 10. The plot shows the total magnification $\mu_{\rm tot}$ against the plasma parameter ω_p^2/ω^2 for different values of β (left panel) and Q (right panel) while keeping fixed $b = 6M$.

We further explore $(\theta_E^{\rm pl})_{\rm uni}$ numerically. Here, the images $(\mu_+^{\rm pl})_{\rm uni}$ and $(\mu_-^{\rm pl})_{\rm uni}$ are defined by

$$(\mu_+^{\rm pl})_{\rm uni} = \frac{1}{4}\left(\frac{x_{\rm uni}}{\sqrt{x_{\rm uni}^2+4}} + \frac{\sqrt{x_{\rm uni}^2+4}}{x_{\rm uni}} + 2\right), \tag{43}$$

and

$$(\mu_-^{\rm pl})_{\rm uni} = \frac{1}{4}\left(\frac{x_{\rm uni}}{\sqrt{x_{\rm uni}^2+4}} + \frac{\sqrt{x_{\rm uni}^2+4}}{x_{\rm uni}} - 2\right), \tag{44}$$

with

$$x_{\rm uni} = \frac{\beta}{(\theta_{\rm E}^{\rm pl})_{\rm uni}}. \tag{45}$$

In figure 10, we plotted the total magnification of the image $\mu_{\rm tot}^{\rm pl}$ in the presence of uniform plasma that exists in the BH environment in the EMS theory for various values of β in the left panel while Q in the right panel. It is obvious from figure 10 that the curves of the total magnification shift down to its smaller values as the parameter β and the BH charge Q increase. We also plotted the total magnification against x_0 for the uniform plasma having suitable parameters, as shown in the top-left panel of figure 12. We explicitly show in figure 12 that the total magnification shifts towards up to its larger magnitude with the increase in the uniform plasma parameters while keeping fixed b/M.

4.2. Non-uniform plasma

Here, we consider non-uniform plasma (as SIS medium) and examine its effect on magnification. For non-uniform plasma it is given by

$$(\mu_{\rm tot}^{\rm pl})_{\rm SIS} = (\mu_+^{\rm pl})_{\rm SIS} + (\mu_-^{\rm pl})_{\rm SIS} = \frac{x_{\rm SIS}^2+2}{x_{\rm SIS}\sqrt{x_{\rm SIS}^2+4}}, \tag{46}$$

with

$$(\mu_+^{\rm pl})_{\rm SIS} = \frac{1}{4}\left(\frac{x_{\rm SIS}}{\sqrt{x_{\rm SIS}^2+4}} + \frac{\sqrt{x_{\rm SIS}^2+4}}{x_{\rm SIS}} + 2\right), \tag{47}$$

$$(\mu_-^{\rm pl})_{\rm SIS} = \frac{1}{4}\left(\frac{x_{\rm SIS}}{\sqrt{x_{\rm SIS}^2+4}} + \frac{\sqrt{x_{\rm SIS}^2+4}}{x_{\rm SIS}} - 2\right), \tag{48}$$

where $x_{\rm SIS}$ is

$$x_{\rm SIS} = \frac{\beta}{(\theta_{\rm E}^{\rm pl})_{\rm SIS}}.$$

By equation (46), one is able to determine the total magnification as a function of the plasma parameter. It can be

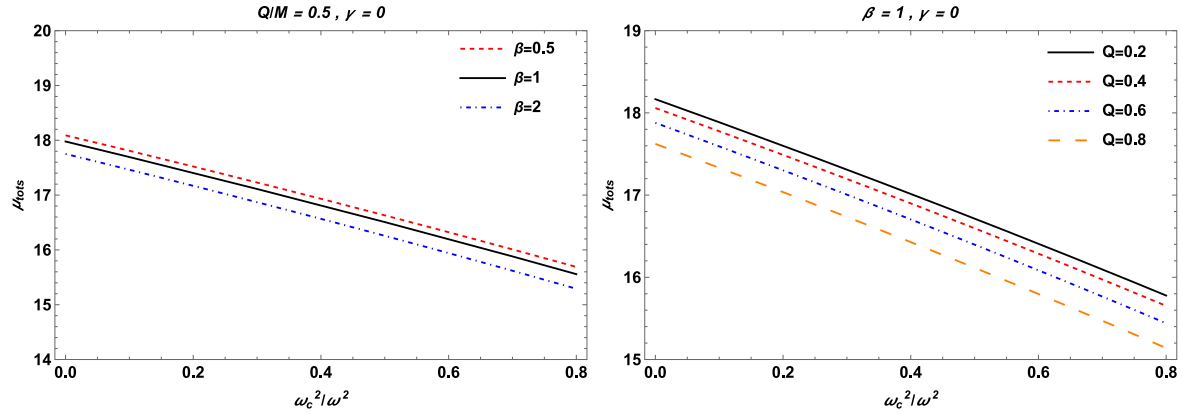

Figure 11. The plot shows the total magnification $\mu_{\rm tots}$ against the plasma parameters ω_c^2/ω^2 for different values of β (left panel) and Q (right panel) while keeping fixed $b = 6M$.

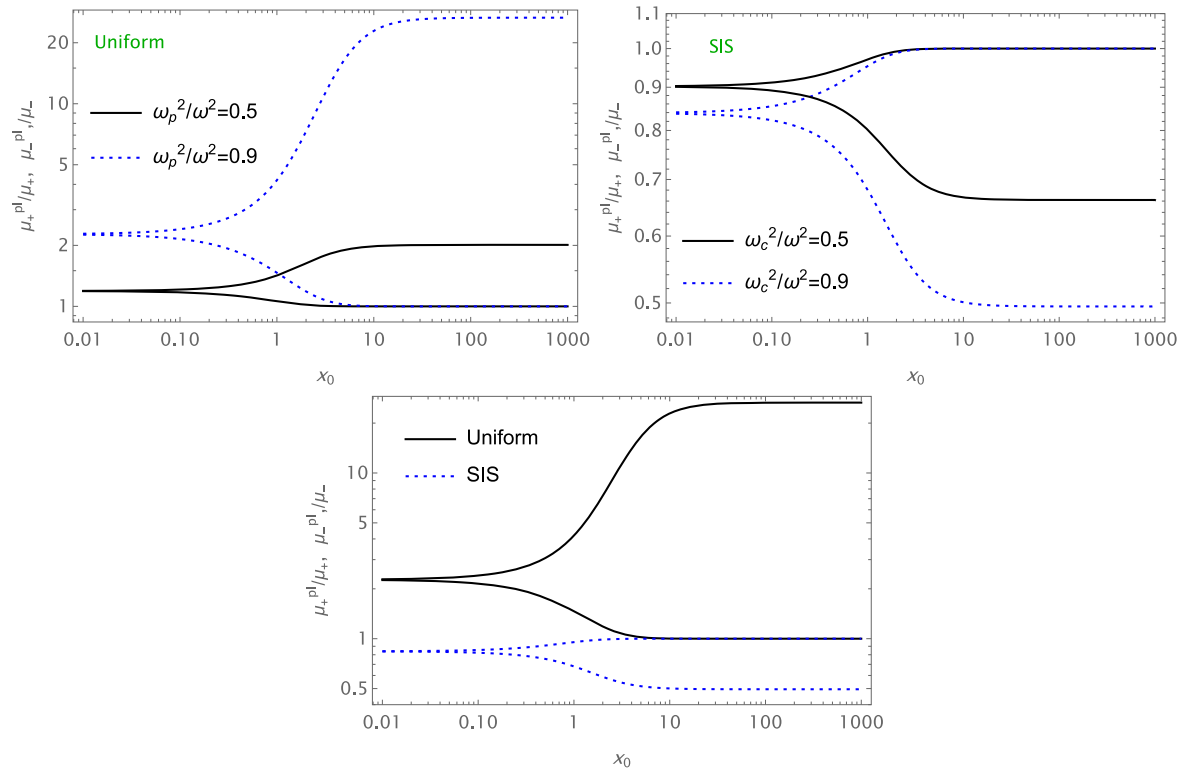

Figure 12. The profile of the image of magnification against x_0. Top-left/right panel: the magnification is plotted under the effect of uniform/SIS. Bottom panel: the comparison of magnification is plotted for uniform and non-uniform plasma cases for the fixed $\omega_{\rm p}^2/\omega^2 = \omega_{\rm p}^2/\omega^2 = 0.9$. We note that we have set $b/M = 3$, $\beta = 1$ and $\gamma = 0$.

observed from figure 11 that the magnification decreases with the increase of the plasma parameter, while its shape also shifts down to its small values as a consequence of β and Q. Furthermore, we also plotted the profile of total magnification as a function of x_0 under the effect of non-uniform plasma while keeping fixed the impact parameter b and the BH parameters, see in the top-right panel of figure 12. Interestingly, we observe that the total magnification decreases under the impact of non-uniform plasma in comparison with one for the uniform plasma. To understand more deeply, we also provide a comparison of uniform and non-uniform plasma cases, which is shown in the bottom panel of figure 12. It can clearly be seen from the comparison that the magnification of uniform plasma distribution is more sensitive than the non-uniform plasma one, i.e. the uniform plasma distribution is larger than the non-uniform plasma one.

5. Conclusions

In this paper, we have investigated the optical properties of the BH in the EMS theory in the presence of plasma medium for various situations. From the performed research we can summarize our main results as follows:

- We have investigated the photon motion around the BH surrounded by a plasma. We have obtained numerical results on the dependence of the radius of the photon sphere on the plasma frequency (see figure 1). It has been shown that the radius of the photon sphere increases with the increase of the plasma frequency. Also, the value of the photon sphere radius decreases under the influence of the β parameter and the BH charge. The radius of the photon sphere depends on the sign of the γ parameter.
- We have also studied the shadow of the BH in plasma. The radius of the BH shadow has been calculated by numerical method. The dependencies of the radius of the BH shadow on the plasma frequency and BH parameter have been demonstrated in figure 3. One can see from this figure that the radius of the BH shadow decreased with the increase of the plasma parameter. The effects of the parameters β and γ and the BH charge for the BH shadow are the same as for the photon sphere.
- In figure 4, we have demonstrated that the size of the shadow depends on the BH and the gravity theory parameters in the future the obtained results can be applied to the images of Sgr A* and M87* SMBHs to get constraints on EMS gravity parameters. Additionally, the observational data of the gravitational lensing in [106–108] may be further used to get constraints on the spacetime parameters of EMS and get estimation the plasma characteristics.
- Furthermore, weak gravitational lensing for the BH in the EMS theory has been investigated. For this, we considered that the BH is surrounded by uniform and non-uniform plasma. We have found the deflection angle for every case independently. Figures 5 and 6 correspond to the uniform plasma case. We can see from these figures that the value of the deflection angle increases with the increase of the plasma frequency. Also, there is a slight decrease with the increase of the β parameter and the BH charge. The obtained results for the non-uniform plasma case are illustrated in figures 7 and 8. It is clear from these figures that the β parameter and the BH charge have the same effect in the case of non-uniform plasma as in the case of uniform plasma. However, the value of the deflection angle decreases with the increase of the non-uniform plasma frequency.
- In addition, we have compared the deflection angle of light for uniform and non-uniform plasma in figure 9. We can easily see from this figure that the value of the deflection angle of light for uniform plasma is greater than for non-uniform plasma.
- Finally, we have studied the total magnification of the images as a function of uniform and non-uniform plasma, and the dependencies have been plotted in figures 10 and 11. It can be seen from these figures that the value of the total magnification of the image for uniform plasma increased with the increase of plasma parameter and for non-uniform plasma vice versa. Also, we have investigated the image magnification for both cases. The results were demonstrated in figure 12.

From an astrophysical viewpoint, it is important to explore optical phenomena around the BHs in different contexts, including in the EMS theory. That is why investigating a solution describing a charged BH in EMS theory as an extension of the RN solution involving a dilaton field could provide an interesting alternative for testing optical phenomena in strong gravity field regimes. Our findings can enhance our understanding of the optical properties of BHs and provide insights into deviations from other BH solutions in astrophysical observations by studying BHs in the EMS theory with a plasma medium and examining their effects on optical phenomena. These theoretical findings not only contribute to theoretical knowledge but also set the stage for future observational and experimental endeavors to investigate extreme environments around BHs.

Acknowledgments

The research is supported by the National Natural Science Foundation of China under Grant No. 11675143 and the National Key Research and Development Program of China under Grant No. 2020YFC2201503. MA wishes to acknowledge Nazarbayev University for the warm hospitality during his stay in Astana, Kazakhstan.

ORCID iDs

Mirzabek Alloqulov https://orcid.org/0000-0001-5337-7117
Sanjar Shaymatov https://orcid.org/0000-0002-5229-7657
Abdul Jawad https://orcid.org/0000-0001-5249-803X

References

[1] Abbott B P *et al* (Virgo and LIGO Scientific Collaborations) 2016 Observation of gravitational waves from a binary black hole merger *Phys. Rev. Lett.* **116** 061102
[2] Abbott B P *et al* (Virgo and LIGO Scientific Collaborations) 2016 Properties of the binary black hole merger *Phys. Rev. Lett.* **116** 241102
[3] Akiyama K *et al* (Event Horizon Telescope Collaboration) 2019 First M87 event horizon telescope results. I. The shadow of the supermassive black hole *Astrophys. J.* **875** L1
[4] Akiyama K *et al* (Event Horizon Telescope Collaboration) 2019 First M87 event horizon telescope results. VI. The shadow and mass of the central black hole *Astrophys. J.* **875** L6
[5] Bambi C 2017 Testing black hole candidates with electromagnetic radiation *Rev. Mod. Phys.* **89** 025001
[6] Walton D J, Nardini E, Fabian A C, Gallo L C and Reis R C 2013 Suzaku observations of 'bare' active galactic nuclei *Mon. Not. R. Astron. Soc.* **428** 2901
[7] Patrick A R *et al* 2011 Iron line profiles in Suzaku spectra of bare Seyfert galaxies *Mon. Not. R. Astron. Soc.* **411** 2353
[8] Patrick A R, Reeves J N, Lobban A P, Porquet D and Markowitz A G 2011 Assessing black hole spin in deep Suzaku observations of Seyfert 1 AGN *Mon. Not. R. Astron. Soc.* **416** 2725
[9] Tan Y, Wang J X, Shu X W and Zhou Y 2012 A possible ultra strong and broad Fe Kα emission line in Seyfert 2 galaxy IRAS 00 521-7054 *Astrophys. J.* **747** L11

[10] Gallo L C *et al* 2011 Multi-epoch X-ray observations of the Seyfert 1.2 galaxy Mrk 79: bulk motion of the illuminating X-ray source *Mon. Not. R. Astron. Soc.* **411** 607
[11] Zajacek M and Tursunov A 2019 The electric charge of black holes: is it really always negligible *The Observatory* **139** 231
[12] Bally J and Harrison E R 1978 The electrically polarized universe *Astrophys. J.* **220** 743
[13] Weingartner J C, Draine B T and Barr D K 2006 Photoelectric emission from dust grains exposed to extreme ultraviolet and x-ray radiation *Astrophys. J.* **645** 1188
[14] Wald R M 1974 Black hole in a uniform magnetic field *Phys. Rev.* D **10** 1680
[15] Kasuya M 1982 Exact solution of a rotating dyon black hole *Phys. Rev.* D **25** 995
[16] Shaymatov S, Sheoran P, Becerril R, Nucamendi U and Ahmedov B 2022 Efficiency of Penrose process in spacetime of axially symmetric magnetized Reissner-Nordström black hole *Phys. Rev.* D **106** 024039
[17] Bardeen J M 1968 *Proc. Int. Conf. GR5, Tbilisi* vol. 174 174
[18] Ayon-Beato E and Garcia A 1999 Non-singular charged black hole solution for non-linear source *Gen. Relativ. Gravitation* **31** 629
[19] Bronnikov K A 2001 Regular magnetic black holes and monopoles from nonlinear electrodynamics *Phys. Rev.* D **63** 044005
[20] Bambi C and Modesto L 2013 Rotating regular black holes *Phys. Lett.* B **721** 329
[21] Fan Z-Y and Wang X 2016 Construction of regular black holes in general relativity *Phys. Rev.* D **94** 124027
[22] Balart L, Panotopoulos G and Rincón 2023 Regular charged black holes, energy conditions, and quasinormal modes *Fortschr. Phys.* **71** 2300075
[23] Rincon A and Gómez G 2023 Quasinormal modes and shadow in Einstein Maxwell Power-Yang-Mills black hole *Phys. Dark Univ.* **46** 101576
[24] Balart L, Belmar-Herrera S, Panotopoulos G and Rincón Á 2023 Novel charged black hole solutions of Born–Infeld type: general properties, Smarr formula and quasinormal frequencies *Ann. Phys.* **454** 169329
[25] Kruglov S I 2023 Magnetically charged AdS black holes and Joule–Thomson expansion *Gravit. Cosmol.* **29** 57
[26] Panotopoulos G 2020 Quasinormal modes of charged black holes in higher-dimensional Einstein-Power-Maxwell theory *Axioms* **9** 33
[27] Rincón Á and Panotopoulos G 2018 Quasinormal modes of scale dependent black holes in (1+2)-dimensional Einstein-Power-Maxwell theory *Phys. Rev.* D **97** 024027
[28] Green M B, Schwarz J H and Witten E 1987 *Superstring Theory. Volume 1—Introduction* (*Cambridge Monographs on Mathematical Physics*) (Cambridge: Cambridge University Press)
[29] Gibbons G and ichi Maeda K 1988 Black holes and membranes in higher-dimensional theories with dilaton fields *Nucl. Phys.* B **298** 741
[30] Garfinkle D, Horowitz G T and Strominger A 1991 Charged black holes in string theory *Phys. Rev.* D **43** 3140
[31] Koikawa T and Yoshimura M 1987 Dilaton fields and event horizon *Phys. Lett.* B **189** 29
[32] Brill D. and Horowitz G. T. 1991 Negative energy in string theory *Phys. Lett.* B **262** 437
[33] Harms B and Leblanc Y 1992 Statistical mechanics of black holes *Phys. Rev.* D **46** 2334
[34] Rakhmanov M 1994 Dilaton black holes with electric charge *Phys. Rev.* D **50** 5155
[35] Gubser S, Klebanov I and Polyakov A 1998 Gauge theory correlators from non-critical string theory *Phys. Lett.* B **428** 105
[36] Witten E 1998 Anti de sitter space and holography *Adv. Theor. Math. Phys.* **2** 253–91
[37] Maldacena J 1999 The large-N limit of superconformal field theories and supergravity *Int. J. Theor. Phys.* **38** 1113
[38] Aharony O, Gubser S S, Maldacena J, Ooguri H and Oz Y 2000 Large *N* field theories, string theory and gravity *Phys. Rep.* **323** 183
[39] Klemm D and Sabra W 2001 Charged rotating black holes in 5d Einstein–Maxwell–(A)dS gravity *Phys. Lett.* B **503** 147
[40] Koch B and Saueressig F 2014 Black holes within asymptotic safety *Int. J. Mod. Phys.* A **29** 1430011
[41] Rincón Á *et al* 2017 Scale-dependent three-dimensional charged black holes in linear and non-linear electrodynamics *Eur. Phys. J.* C **77** 494
[42] Koch B, Reyes I A and Rincón 2016 A scale dependent black hole in three-dimensional space–time *Class. Quantum Gravity* **33** 225010
[43] Bonanno A, Khosravi A-P and Saueressig F 2021 Regular black holes with stable cores *Phys. Rev.* D **103** 124027
[44] Bonanno A and Saueressig F 2022 *Stability Properties of Regular Black Holes* (Singapore: Springer Nature)
[45] Synge J 1966 The escape of photons from gravitationally intense stars *Mon. Not. R. Astron. Soc.* **131** 463
[46] Luminet J 1979 The escape of photons from gravitationally intense stars *Astron. Astrophys.* **75** 228–35
[47] Amarilla L and Eiroa E F 2013 Shadow of a Kaluza-Klein rotating dilaton black hole *Phys. Rev.* D **87** 044057
[48] Wei S-W and Liu Y-X 2013 Observing the shadow of Einstein-Maxwell-Dilaton-Axion black hole *JCAP* **11** 063
[49] Badí J and Eiroa E F 2023 Shadows of rotating Einstein-Maxwell-dilaton black holes surrounded by a plasma *Phys. Rev.* D **107** 124028
[50] Konoplya R A and Zhidenko A 2021 Shadows of parametrized axially symmetric black holes allowing for separation of variables *Phys. Rev.* D **103** 104033
[51] Rosa J L and Rubiera-Garcia D 2022 Shadows of boson and Proca stars with thin accretion disks *Phys. Rev.* D **106** 084004
[52] Rosa J L, Macedo C F and Rubiera-Garcia D 2023 Imaging compact boson stars with hot spots and thin accretion disks *Phys. Rev.* D **108** 044021
[53] Rosa J L 2023 Observational properties of relativistic fluid spheres with thin accretion disks *Phys. Rev.* D **107** 084048
[54] Kumar S G G R and Singh B P 2018 Shadow and deflection angle of rotating black hole in asymptotically safe gravity *Ann. Phys.* **420** 168252
[55] Konoplya R A 2019 Shadow of a black hole surrounded by dark matter *Phys. Lett.* B **795** 1–6
[56] Vagnozzi S and Visinelli L 2019 Hunting for extra dimensions in the shadow of M87* *Phys. Rev.* D **100** 024020
[57] Kumar R and Ghosh S G 2020 D→4 Einstein-Gauss-Bonnet gravity and beyond *JCAP* **2020** 7
[58] Afrin M, Kumar R and Ghosh S G 2021 Parameter estimation of hairy Kerr black holes from its shadow and constraints from M87* *Mon. Not. R. Astron. Soc.* **504** 5927
[59] Abdujabbarov A, Amir M, Ahmedov B and Ghosh S G 2016 Shadow of rotating regular black holes *Phys. Rev.* D **93** 104004
[60] Zhang M and Guo M 2020 Can shadows reflect phase structures of black holes? *Eur. Phys. J.* C **80** 790
[61] Konoplya R A and Zhidenko A 2019 Analytical representation for metrics of scalarized Einstein-Maxwell black holes and their shadows *Phys. Rev.* D **100** 044015
[62] Mustafa G, Atamurotov F, Hussain I, Shaymatov S and Övgün A 2022 Shadows and gravitational weak lensing by the Schwarzschild black hole in the string cloud background with quintessential field *Chin. Phys.* C **46** 125107
[63] Tsukamoto N, Li Z and Bambi C 2014 Constraining the spin and the deformation parameters from the black hole shadow *J. Cosmol. Astropart. Phys.* **2014** 043–043
[64] Tsukamoto N 2018 Black hole shadow in an asymptotically flat, stationary, and axisymmetric spacetime: the Kerr-Newman and rotating regular black holes *Phys. Rev.* D **97** 064021

[65] Eslam Panah B, Jafarzade K and Hendi S 2020 Charged 4D Einstein-Gauss-Bonnet-AdS black holes: shadow, energy emission, deflection angle and heat engine *Nucl. Phys.* B **961** 115269

[66] Olmo G J, Rosa J L, Rubiera-Garcia D and Sáez-Chillón Gómez D 2023 Shadows and photon rings of regular black holes and geonic horizonless compact objects *Classical Quantum Gravity* **40** 174002

[67] Asuküla H *et al* 2023 Spherically symmetric vacuum solutions in 1-parameter new general relativity and their phenomenology *Phys. Rev.* D **109** 064027

[68] Al-Badawi A, Alloqulov M, Shaymatov S and Ahmedov B 2024 Shadows and weak gravitational lensing by the black hole in Einstein-Maxwell-scalar theory *Chin. Phys.* C **48** 095105

[69] Albadawi A, Shaymatov S, Alloqulov M and Wang A 2024 A regular MOG black hole's impact on shadows and gravitational weak lensing in the presence of quintessence field *Commun. Theor. Phys.* **76** 085401

[70] Eddington A S 1919 The total eclipse of 1919 May 29 and the influence of gravitation on light *The Observatory* **42** 119

[71] Morozova V S, Ahmedov B J and Tursunov A A 2013 Gravitational lensing by a rotating massive object in a plasma *Astrophys. Space Sci.* **346** 513

[72] Bisnovatyi-Kogan G S and Tsupko O Y 2010 Gravitational lensing in a non-uniform plasma *Mon. Not. R. Astron. Soc.* **404** 1790

[73] Tsupko O Y and Bisnovatyi-Kogan G S 2012 On gravitational lensing in the presence of a plasma *Gravitation Cosmol.* **18** 117

[74] Cunha P V P, Eiró N A, Herdeiro C A R and Lemos J P S 2020 Lensing and shadow of a black hole surrounded by a heavy accretion disk *J. Cosmol. A. P* **2020** 035

[75] Babar G Z, Atamurotov F and Babar A Z 2021 Gravitational lensing in 4-D Einstein-Gauss-Bonnet gravity in the presence of plasma *Phys. Dark Uni.* **32** 100798

[76] Javed W, Atique M and Övgün A 2022 Probing effective loop quantum gravity on weak gravitational lensing, Hawking radiation and bounding greybody factor by black holes *Gen. Relativ. Gravit.* **54** 135

[77] Jafarzade K, Kord Zangeneh M and Lobo F S N 2021 Shadow, deflection angle and quasinormal modes of Born-Infeld charged black holes *J. Cosmol. A. P.* **2021** 008

[78] Atamurotov F, Ortiqboev D, Abdujabbarov A and Mustafa G 2022 Particle dynamics and gravitational weak lensing around black hole in the Kalb-Ramond gravity *Eur. Phys. J.* C **82** 659

[79] Atamurotov F, Shaymatov S and Ahmedov B 2021 Particle motion and plasma effects on gravitational weak lensing in Lorentzian wormhole spacetime *Galaxies* **9** 54

[80] Atamurotov F, Shaymatov S, Sheoran P and Siwach S 2021 Charged black hole in 4D Einstein-Gauss-Bonnet gravity: particle motion, plasma effect on weak gravitational lensing and centre-of-mass energy *J. Cosmol. Astrophys.* **2021** 045

[81] Rogers A 2015 Frequency-dependent effects of gravitational lensing within plasma *Mon. Not. R. Astron. Soc.* **451** 17

[82] Babar G Z, Babar A Z and Atamurotov F 2020 Optical properties of Kerr-Newman spacetime in the presence of plasma *Eur. Phys. J. C.* **80** 761

[83] Javed W, Riaz S, Pantig R C and Övgün A 2022 Weak gravitational lensing in dark matter and plasma mediums for wormhole-like static aether solution *Eur. Phys. J.* C **82** 1057

[84] Javed W, Hussain I and Övgün A 2022 Weak deflection angle of Kazakov-Solodukhin black hole in plasma medium using Gauss-Bonnet theorem and its greybody bonding *Eur. Phys. J. Plus* **137** 148

[85] Benavides-Gallego C, Abdujabbarov A and Bambi C 2018 Gravitational lensing for a boosted Kerr black hole in the presence of plasma *Eur. Phys. J. C.* **78** 694

[86] Atamurotov F, Alloqulov M, Abdujabbarov A and Ahmedov B 2022 Testing the Einstein-Æther gravity: particle dynamics and gravitational lensing *Eur. Phys. J. Plus* **137** 634

[87] Jiang H, Alloqulov M, Wu Q, Shaymatov S and Zhu T 2024 Periodic orbits and plasma effects on gravitational weak lensing by self-dual black hole in loop quantum gravity *Phys. Dark Univ.* **46** 101627

[88] Övgün A, Sakallı İ and Saavedra J 2019 Weak gravitational lensing by Kerr-MOG black hole and Gauss-Bonnet theorem *Ann. Phys.* **411** 167978

[89] Rahvar S and Moffat J W 2019 Propagation of electromagnetic waves in MOG: gravitational lensing *Mon. Not. R. Astron. Soc.* **482** 4514

[90] Izmailov R N, Karimov R K, Zhdanov E R and Nandi K K 2019 Modified gravity black hole lensing observables in weak and strong field of gravity *MNRAS* **483** 3754

[91] Yu S, Qiu J and Gao C 2021 Constructing black holes in Einstein–Maxwell-Scalar theory *Classical Quantum Gravity* **38** 105006

[92] Gao C J and Zhang S N 2004 Dilaton black holes in the de Sitter or anti de Sitter universe *Phys. Rev.* D **70** 124019

[93] Kurbonov N *et al* 2023 Charged particles and penrose process near charged black holes in Einstein-Maxwell-Scalar theory *Eur. Phys. J.* C **83** 506

[94] Alloqulov M, Shaymatov S, Ahmedov B and Jawad A 2024 Radiation properties of the accretion disk around a black hole in Einstein-Maxwell-Scalar theory *Chin. Phys.* C **48** 025101

[95] Synge J L 1960 *Relativity: The General Theory* (Amsterdam: North-Holland)

[96] Tsupko O Y and Bisnovatyi-Kogan G S 2009 Relativistic rings due to Schwarzschild gravitational lensing *Gravit. Cosmol.* **15** 184

[97] Perlick V, Tsupko O Y and Bisnovatyi-Kogan G S 2015 Influence of a plasma on the shadow of a spherically symmetric black hole *Phys. Rev.* D **92** 104031

[98] Rogers A 2015 Frequency-dependent effects of gravitational lensing within plasma *Mon. Not. R. Astron. Soc.* **451** 17

[99] Akiyama K *et al* (Event Horizon Telescope Collaboration) 2021 First M87 Event Horizon Telescope Results. VII. Polarization of the Ring *Astrophys. J.* **910** L12

[100] Bambi C, Freese K, Vagnozzi S and Visinelli L 2019 Testing the rotational nature of the supermassive object M87* from the circularity and size of its first image *Phys. Rev.* D **100** 044057

[101] Bisnovatyi-Kogan G S and Tsupko O Y 2010 Gravitational lensing in a non-uniform plasma *Mon. Not. R. Astron. Soc.* **404** 1790

[102] Bozza V 2008 Comparison of approximate gravitational lens equations and a proposal for an improved new one *Phys. Rev.* D **78** 103005

[103] Atamurotov F, Abdujabbarov A and Rayimbaev J 2021 Weak gravitational lensing Schwarzschild-Mog black hole in plasma *Eur. Phys. J.* C **81** 118

[104] Alloqulov M, Atamurotov F, Abdujabbarov A and Ahmedov B 2023 Probing Hořava-Lifshitz gravity using particle and photon dynamics in the presence of plasma *Chin. Phys.* C **47** 075103

[105] Alloqulov M, Atamurotov F, Abdujabbarov A, Ahmedov B and Khamidov V 2024 Shadow and weak gravitational lensing for Ellis-Bronnikov wormhole* *Chin. Phys.* C **48** 025104

[106] Wang Y 2005 Observational signatures of the weak lensing magnification of supernovae *JCAP* **2005** 005

[107] Gonzalez E J *et al* 2015 Low X-ray luminosity galaxy clusters —III. Weak lensing mass determination at $0.18 < z < 0.70$ *MNRAS* **452** 2225

[108] Kalantari Z, Rahvar S and Ibrahim A 2022 Fermi-GBM observation of GRB 090 717 034: χ^2 test confirms evidence of gravitational lensing by a supermassive black hole with a million solar mass *Astrophys. J.* **934** 106